Datasets of Long Range Navigation Experiments in a Moon Analogue Environment on Mount Etna

Mallikarjuna Vayugundla, Florian Steidle, Michal Smisek, Martin J. Schuster, Kristin Bussmann, and Armin Wedler
German Aerospace Center (DLR), Robotics and Mechatronics Center (RMC), Münchner Str. 20, D-82234 Wessling, Germany

Abstract

Long range navigation capabilities are crucial to increase the level of autonomy for robotic planetary exploration missions. As the opportunities to collect data on the surfaces of other planets are both very limited and expensive, space analogue sites on Earth play an important role to develop and test robotic systems. We provide and present two datasets captured with our Lightweight Rover Unit (LRU) at a planetary surface analogue test site on Mt. Etna, Sicily, Italy. In distinction to many other robot navigation datasets, we were able to capture datasets in an environment that is in terms of its visual and terramechanical properties close to the character of surfaces of rocky planets, hence making our data valuable for the development of visual-inertial navigation systems for planetary and unstructured GPS-denied outdoor environments. We make both of our datasets publicly available and free to download for other researchers to use them to test, improve and evaluate their navigation methods. We provide raw data in the form of ROS bagfiles containing gray-scale images, dense depth images, sensor readings from an Inertial Measurement Unit (IMU) and wheel odometry estimates. In addition, the data contains ground truth for the rover trajectory obtained via differential GPS (DGPS) to allow an evaluation of robot localization methods. The datasets were recorded during experiments, in which our rover traversed paths of approximately 1 km in length each. This makes them useful for testing pose estimation methods over long ranges.

1 INTRODUCTION

Mobile robots are nowadays being deployed in situations, in which human presence is required, but it would be dangerous or impossible. Planetary exploration or disaster relief are examples of such scenarios. Mobile robotics systems are being developed in laboratory conditions, which always limit the testability of their intended use-cases. Should these systems and methods not deviate from original specifications, they need to be tested in application-relevant analogous environments. However, it can be demanding and expensive to physically conduct an analogous test there. In these instances, datasets collected from previous well-designed experiments can provide invaluable means to test novel navigation methods, without asking its developer to absolve an actual field test physically anew.

There have been projects contributing valuable navigation datasets to the scientific community, e.g. by ESA [1], Autonomous Systems Lab, ETH Zurich [2]. The latter have also put together a list of other such efforts by various institutes and universities [3]. Another such collection is listed by OpenSLAM [4].

However, we know of very few publications, where authors have conducted a field test in a planetary-analogous scenario with a robotic demonstrator, managing to capture relevant datasets and sharing them publicly. This is surprising, given how the lack of autonomous navigation over long ranges hinders the scientific yield of current-generation planetary exploration missions. Among those few publications that try to overcome this, we mention [5] whose authors publish a dataset of a planetary rover captured on a beach near Katwijk, Netherlands. Similarly, a publication [6] whose main goal was to demonstrate importance of visual odometry in robotic planetary exploration missions, also provides datasets captured by a planetary rover system in the Atacama desert in Chile.

Figure 1 LRU at the experiment site on Mt. Etna, Italy
P.C: Esther Horvath

We provide two similar long range datasets captured by Lightweight Rover Unit (LRU) on Mt. Etna in Sicily. In **Figure 1** you can see a photo of LRU on Mt. Etna, performing its mission.

In this publication, we describe an experiment conducted by a planetary rover prototype in a planetary-analogue en-

ISBN 978-3-8007-4699-6

vironment, primary goal of which was to capture the long range navigation datasets to evaluate localization and mapping methods intended to be used in next-generation planetary rovers. To achieve this goal, great care has been taken to assure time synchronization, correct sensor data time stamping, calibration and complete transformation tree. DGPS is used as localization ground truth. As a result, the datasets presented contain synchronized, consistent and continuous data. Up to our knowledge, these are the first published datasets of such completeness. We provide the two datasets publicly for download, in order to allow other researchers to evaluate their localization and mapping methods.

In upcoming sections, we will describe in more detail the test site, the demonstrator, the format and contents of captured datasets. We will focus on explaining their relevance as planetary exploration mission analogue. Then, we will present evaluation of our navigation chain using these datasets.

2 SCENARIO OVERVIEW

Datasets were captured on Mount Etna, Italy, during the final demonstration of ROBEX mission [7, 8] in June and July 2017. While Mt. Etna was chosen to be a highly-representative Moon analogue site for purposes of ROBEX mission mainly due to its seismic activities, the long range navigation experiment benefited from the presence of fine grain lava soil, which is in grain size and mineralogical context comparable to areas of the Martian surface [9]. This terrain's visual appearance and terramechanical properties make it an ideal analogue for rocky planet surfaces. Furthermore, the test site situated at 2600m a.s.l. provides an environment with a negligible amount of vegetation, low humidity and clear illumination conditions, adding to the representativeness of datasets captured there.

3 SYSTEM OVERVIEW

Datasets were captured by LRU [10], a four-wheeled space rover prototype designed for autonomous operations in GPS-denied environments[11]. LRU was built by the Institute of Robotics and Mechatronics, DLR. The sensor suite of LRU used for navigation purposes consists of a stereo camera bench mounted on a pan-tilt unit, an inertial measurement unit (IMU), and a wheel odometry based on wheel encoder readings. LRU is equipped with a differential GPS module, which, together with a reference DGPS station, provided ground truth of the robot's position with an accuracy of few centimeters. The complete sensor data acquisition and processing is done on-board the rover. It is equipped with a an Intel Core i7-3740QM CPU for computation. It also has a Spartan-6 FPGA board in addition to the CPU to calculate depth images.

Additionally, LRU carries an Intel Atom E3845 CPU to perform the real time control of the manipulator and the body. Also, the camera sensor unit contains five additional cameras used for scientific purposes - a color camera, a thermal camera, a high resolution camera and a wide-baseline stereo camera bench with a set of multispectral filters. These additional sensors are not used for navigation purposes and their sensor readings are not included in the datasets.

The system architecture diagram presenting the flow of sensor data processed by software components in order to compute the robot's localization state, as well as a parallel processing chain capturing DGPS-based localization ground truth, is shown in **Figure 2**. The details of the sensors, their calibration, sensor-data processing by our perception and localization components and recorded data along with the processing of GNSS data for ground truth are explained in the following sections.

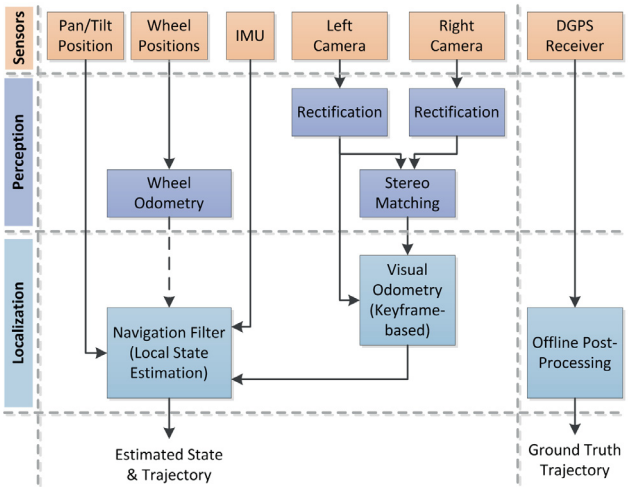

Figure 2 System architecture

3.1 Sensor Setup

This section describes sensors in more detail. Inertial measurement unit (IMU) is located in the center of the rover body. Its axes define the reference frame of the rover, **Figure 3**. Additionally, two grayscale cameras are mounted on a pan-tilt unit. The cameras have a baseline of ≈ 9 cm. Based on their images, depth images are calculated. To transform data from the camera frame to the imu frame, the static transformations $T_{\text{imu}}^{\text{pt,base}}$ and $T_{\text{cam,left}}^{\text{pt}}$ are given by calibration. The transformation $T_{\text{pt,base}}^{\text{pt}}$ is determined online based on encoder readings. The readings from the wheel encoders and the steering angle of each wheel are used to calculate a wheel odometry and transform it to the imu frame. The DGPS antenna is mounted on an additional support. Its position was extracted from CAD data. An overview of sensors used is given in **Table 1**. For some sensors, e.g. cameras, raw data is provided in the datasets. The readings from other sensors, e.g. encoders, are preprocessed and only the results are part of the datasets.

3.2 Sensor Calibration

Calibration of the stereo camera bench is performed using DLR-proprietary solutions, CalDe and CalLab [12]. A chessboard-like 2D calibration target is used. CalDe is used to extract correspondences between the known relative positions of target's corners and their positions de-

Sensor	Description	Data
Navigation Cameras	AlliedVision Mako G-125	monochrome 1292x964 px images
Imu	XSENS MTi-10 IMU	three-axis acceleration and angular rates
Wheel Encoder	Digital Hall-Sensor	4200 increments/joint rotation
Pan-Tilt Encoder	Digital Hall-Sensor	4200 increments/joint rotation
Body Encoder	Digital Hall-Sensor	4200 increments/joint rotation
DGPS	Piksi Multi GNSS Module by Swift Navigation	GNSS Data

Table 1 Main sensors used on LRU to collect the datasets.

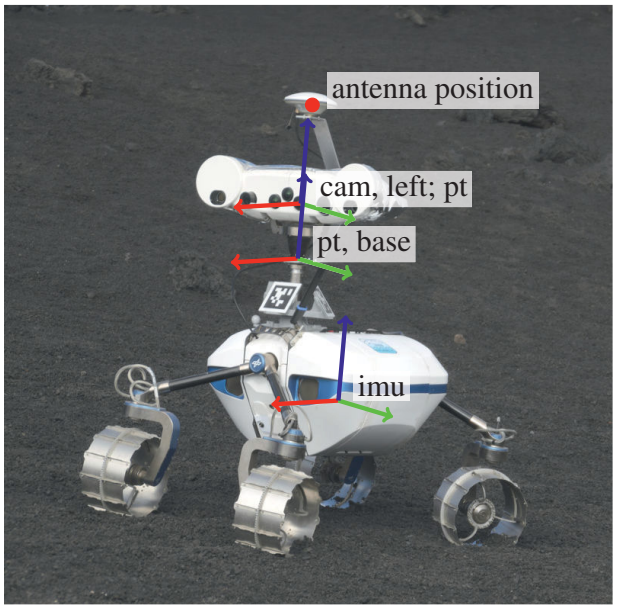

Figure 3 Main coordinate frames on LRU. In the depicted configuration the cam, left frame and pan-tilt frame almost coincide. Therefore only one coordinate frame is shown.

tected in images of it captured by the cameras being calibrated. CalLab is used to compute intrinsic and extrinsic parameters of these cameras via non-linear optimization.
Two calibration datasets were captured. In the first of those, multiple images of a calibration target were captured by rover's cameras. During this procedure, the rover was kept motionless and the calibration target was captured from various poses. This dataset was used to obtain intrinsic parameters, distortion parameters (two radial distortion parameters released) and the 6DOF stereo camera baseline $T_{\text{cam,left}}^{\text{cam,right}}$. In capturing the second dataset, the calibration target was kept static and the pan and tilt angles of the pan-tilt unit were changed. For each shot captured, these pan and tilt values were stored. Based upon this dataset and the results of the previous calibration step, the 6DOF transformation between the left camera and the rotational center of pan-tilt unit, $T_{\text{pt}}^{\text{cam,left}}$, was computed.
Then, the rover was lifted and subjected to the rotational motion. During this process, visual odometry and gyroscope measurements from IMU were captured. These two sources of information were used to calibrate the rotational part of the the imu to camera transformation using the method described in [13] and [14]. This procedure yields refined rotation of $T_{\text{imu}}^{\text{cam,left}}$, from which, given that $T_{\text{pt}}^{\text{cam,left}}$ and $T_{\text{pt,base}}^{\text{pt}}$ are known, rotation of $T_{\text{imu}}^{\text{pt,base}}$ is computed and stored. The translational part of this transformation is taken from the CAD model and is centimetre-accurate, and is not further refined.
Intrinsic calibration is needed for the image rectification process. Extrinsic calibration is required to describe rover's transformation tree. We consider the calibration results to be an important supplementary material for those interested to use our long range navigation datasets to evaluate their localization and mapping solutions. Therefore, we provide them as well, alongside with the main datasets.

4 DATASETS

The two datasets were collected during the ROBEX demo mission space campaign, which took place in June and July 2017 at Mount Etna. The datasets contain information needed to develop and test algorithms in the field of localization, navigation and stereo-vision based mapping. The datasets were collected during two long range navigation experiments, where the rover was operated using a gamepad in order to follow a trajectory of our choice. Ground truth trajectories based on differential GPS data and mapped on the original site using Google Earth are shown in **Figure 4**.
For most of the sensors raw signals were recorded. These include the measurements from the inertial measurement unit, the images (left camera image and depth image) from the stereo-camera setup and control commands sent to the robot. Based on the raw signals of sensors, further calculations are performed. These include a wheel odometry, a visual odometry, non-static transformations between coordinate frames and depth-images.
Wheel odometry is based on the approach described in [15]. For each discrete timestamp t_s it calculates planar linear and angular velocities in the body frame. Linear velocities are calculated in the xy-plane of the body frame (${}^{\text{b}}v_{\text{w}} \in \mathbb{R}^2$) and angular velocity around the z-axis (${}^{\text{b}}\omega_{\text{w}} \in \mathbb{R}$). Based on the depth-images calculated using Semi-Global Matching (SGM) [16] on the LRU's FPGA-board , visual odometry [17] estimates are computed. They consist of the position change $\Delta^{c_{t_s}} p_{c_{t_e}} \in \mathbb{R}^3$ and the orientation change $\Delta^{c_{t_s}} q_{c_{t_e}} \in \mathbb{R}^4$ of the camera between images taken at the two timestamps t_s and t_e. To reduce drift, which is introduced when integrating position and orientation changes, visual odometry is able to use keyframes.

ISBN 978-3-8007-4699-6

Figure 4 Trajectories of the long range navigation tests plotted with Google Earth using the DGPS ground truth data; length of the trajectory of dataset 1 (brown) is approximately 834 m and of trajectory of dataset 2 (black) is approximately 1097 m

The readings from the IMU consist of a timestamp t_s, angular rates ${}^{\mathrm{b}}\omega_{\mathrm{b}} \in \mathbb{R}^3$ and accelerations ${}^{\mathrm{b}}a_{\mathrm{b}} \in \mathbb{R}^3$. An indirect Extended Kalman filter [18] is used to fuse visual and wheel odometry measurements with readings from the IMU. It estimates the position $\hat{p}$, translational velocity $\hat{v}$ and orientation $\hat{q}$ of the body frame with respect to the initial position of the rover. Additionally, the IMU biases $\hat{b}_{\mathrm{a}}$, $\hat{b}_{\omega}$ are estimated.

In order to compute the ground truth we used the Piksi Multi GNSS Modules from Swift Navigation. Using the software tools provided by the vendor, we recorded the satellite data separately on the rover and base-station which is enough to compute the position of the DGPS antenna ${}^{\mathrm{gps}}p_{\mathrm{a}} \in \mathbb{R}^3$ with centimeter-level accuracy. We preferred to collect the GNSS data files separately on the rover and the base station and do off-line processing to compute the DGPS solution as ground truth. This helps us to have no interruptions in the DGPS solution while if you compute the DGPS solution and log it online, any interruptions in Wi-Fi communication will cause loss of quality in the computed DGPS solution which is likely as the rover has moved almost 500 metres away from the control center where the base station is located. For one of the runs (dataset 1 in **Figure 4**) we had an interruption in the collection of the base-station data. Hence, the base-station data is collected as two files with an interruption of 618 seconds i.e. approximately 10.3 minutes in-between. The interruption happened towards the end of the experiment. Hence, we have a loss of quality in the ground truth trajectory for this period as we had only the GNSS data from the rover alone for the period of interruption. We provide both the raw GNSS files recorded on the rover and the base station as well as the computed DGPS solution using those files. Moreover, we also provide the aligned DGPS trajectory with respect to the pose-estimation trajectory of our system using the pipeline described in Section 5.

The datasets are available for public to download at `http://mobilerobots.dlr.de/datasets`. On this page we give additional description of the datasets along with details on how the data is organized.

5 EVALUATION

The datasets and associated metadata available online should contain all the information necessary to test mobile robotics localization and mapping algorithms. Data is time-synchronized, calibrated and full transformation tree is given. We first describe a preprocessing workflow needed to be performed, in order for the user to be able to compare localization results to ground truth and then disseminate preliminary evaluation results for our localization implementation.

5.1 Data Evaluation Methodology

In order to evaluate the performance of pose estimation by comparing it to ground truth, these two information sources need to be registered temporally and spatially. For temporal registration, time-stamp unification, DGPS filtering and data association need to be performed. For spacial registration, frame definition, initial positioning and rotational alignment need to be performed. In the remaining paragraphs of this subsection, these steps will be explained.

DGPS Solution Calculation
We recorded the GNSS data seperately on the rover and a stationary base station. These two files are then used to compute the DGPS solution offline using RTKLIB [19] which is a open-source library for computing DGPS solution from GNSS data both online and offline.

Unified Timestamp Representation
DGPS data contains timestamps from two sources - GPS time and host computer time - for each entry. Pose estimation contains computer time timestamps. Therefore, time-stamp unification is rather trivial - we simply use host computer timestamps.

Qualitative Filtering of DGPS Data
DGPS data contains periods of quality reduction and even of complete signal loss. We only use data entries for which the fixed position is extracted and for which standard deviation is no more than 0.1 m. Other entries are omitted.

Data Association Between Pose Estimation Data and DGPS Data
Pose estimation is given at 80 Hz frequency. DGPS data is given at 10Hz frequency, with the possibility of arbitrarily long blackouts. We consider data entries as fit for associating, once we find pose estimation and DGPS entries that don't differ by more than 0.02 s in their timestamps. For a rover driving at maximum speed 0.2 m/s, using nearest-neighbor interpolation to associate pose estimation and DGPS data introduces a worst-case error of 4 mm. This error is non-cumulative.

Spatial Alignment of Pose Estimation Data and Processed DGPS Data
Pose estimation is given in the robot body frame. DGPS is given in GPS receiver frame, which in our case is posi-

ISBN 978-3-8007-4699-6

tioned above pan-tilt unit. Since DGPS data contains no rotation, location of robot body frame cannot be deduced from this information. Therefore we need to compare the datasets in GPS receiver frame.

Pose estimation is given in initial pose of robot body frame and DGPS is given in absolute geodetic WGS84 (east-north-up). Initial position of robot body frame in WGS84 frame is not known. Due to having already performed the data association, we assume that in the beginning of the run they both start in the same point in space.

Not knowing the initial pose of robot body in WGS84 causes also an issue of not knowing the initial rotation of those two frames. We use the first 4 m of both datasets of a run to rotationally align ground truth to pose estimation. Since both the initial pose estimation and DGPS data are oriented so that z-axis is parallel to gravity vector, a 1DOF rotation - only about z-axis - was sufficient.

5.2 Preliminary Evaluation Results of Our Pose-Estimation System

Using the datastets and the GNSS data files, we evaluated our existing pose estimation system that is running on the rover. For the evaluation we used the steps described in the Section 5.1. We used three error metrics to represent the performance of the pose estimation system as defined below:

Absolute Error

At every time-step in the final trajectories of processed pose estimation output and ground truth, the distance between the estimated position and the ground truth is calculated.

Relative Error

The relative error e_k relates the error between the ground truth position $p_k \in \mathbb{R}^3$ and the estimated position $\hat{p}_k \in \mathbb{R}^3$ to the total length of trajectory for each time step k. It is defined as

$$e_k = \frac{\hat{p}_k - p_k}{\sum_{t=1}^{k} \|p_t - p_{t-1}\|_2} \,. \tag{1}$$

Relative Deviation

The relative deviation d_a relates the estimated length $\hat{s}$ of segments of the trajectory to the calculated length s based on reference data. For a segment length a it is defined as

$$d_a = \frac{\hat{s}_a - s_a}{s_a} \,. \tag{2}$$

Already on the test site, we noticed that a high slip terrain might impede the reliability of wheel odometry significantly. Therefore, in our analysis, we focused on analysing the influence of including wheel odometry or not on the pose estimation.

The pose estimation system had a maximum absolute error of 55.0 m without wheel odometry and 99.9 m with wheel odometry for dataset 1 and 28.7 m without wheel odometry and 72.9 m with wheel odometry for dataset 2. The relative error and relative deviation analysis results for the dataset 1 are in **Figure 5** and dataset 2 are in **Figure 6**.

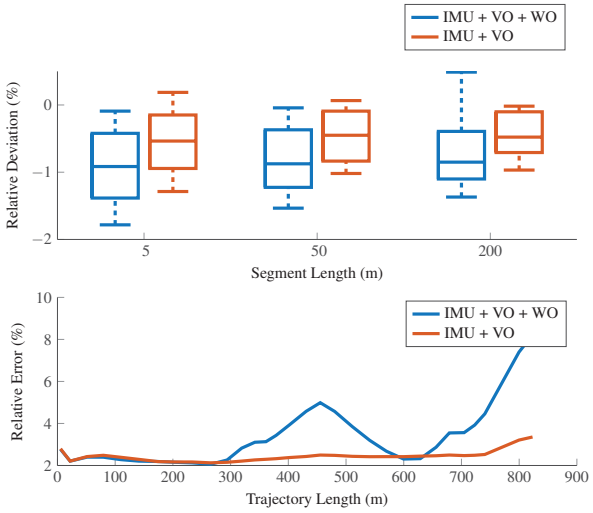

Figure 5 Error for dataset 1; *top*: relative deviation for trajectory segments of 5 m, 50 m and 200 m lengths; *bottom*: relative error in comparison to distance traveled

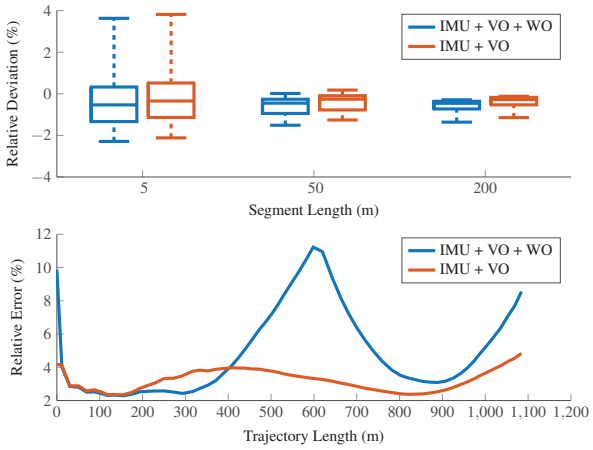

Figure 6 Error for dataset 2; *top*: relative deviation for trajectory segments of 5 m, 50 m and 200 m lengths; *bottom*: relative error in comparison to distance traveled

The relative deviation d_a is smaller for both datasets if wheel odometry is not used to estimate the position $\hat{p}$ of the rover. It is an indication that the assumption of zero-mean Gaussian noise is not true for wheel odometry errors for the whole trajectory. In dataset 2 the turning point is reached after a traveled distance of approximately 600 m, **Figure 6**. Before the turning point, the relative error e increases, if wheel odometry is used. On the other hand in the beginning of dataset 1 a positive influence of wheel odometry on the position estimation is visible.

From the above error analysis, it can be seen that our pose estimation system performs better when wheel odometry is not included. We account this to the challenging terrain on Etna which makes it hard to estimate slip and also that the inclusion of wheel odomtery as input to our pose estimation component is a preliminary recent addition to our system that might require further development and parameter tuning, in particular for a high slip environment. The resulting plots showing the trajectories of the pose estima-

ISBN 978-3-8007-4699-6

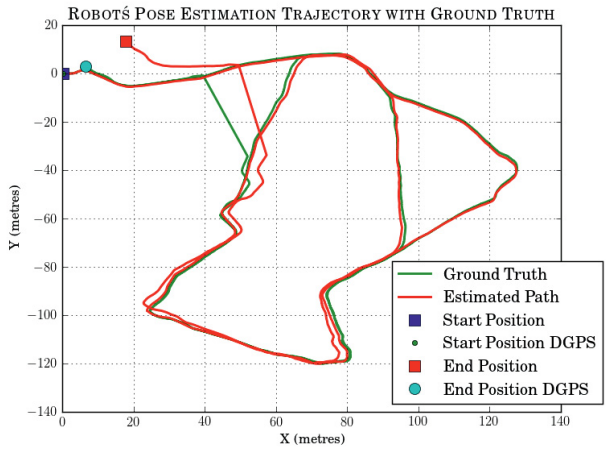

(a)

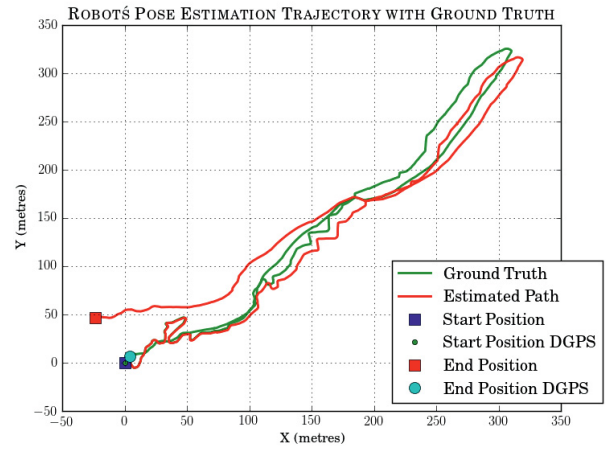

(b)

Figure 7 (a) Pose estimation trajectory and aligned DGPS trajectory for dataset 1. (b) Pose estimation trajectory and aligned DGPS trajectory for dataset 2.

tion output along with temporally and rotationally aligned ground truth that is calculated from the GNSS data are presented in **Figure 7**.

From this preliminary analysis, we noticed significant differences between rover's performance in laboratory conditions and in the field. While the wheel odometry provides almost no slip in laboratory conditions, driving in fine-grained soil makes the wheels slip significantly, limiting the usefulness of the wheel odometry. On the contrary, while visual systems need to face the challenge of reduced illumination, lack of features and light reflections in laboratory conditions, bright light on Mt. Etna with feature-rich and reflection-free terrain make visual odometry a very reliable source of localization information. These findings, in accordance with those of [6], underline the importance of field testing as opposed to laboratory-only experimenting.

6 CONCLUSION

In this article, we introduced two long range datasets, collected in a planetary-analogue environment of Mt. Etna, by the planetary rover prototype LRU, while driving approximately one kilometre. The datasets were collected during the demo mission of the ROBEX project in June and July 2017. We share these two datasets with the robotics community, believing that they will be very helpful to test navigation algorithms aimed for GPS-denied and unstructured outdoor environments, e.g. planetary exploration. Preliminary analysis shows significant difference in the performance of the navigation system between the tests in the laboratory conditions and in the field test. This highlights the need for testing systems and algorithms in their target environments and the value of application-representative datasets. In future work, we plan to provide the tools that we used for processing the pose estimation trajectory and the ground truth data computed from GNSS data to the robotics community.

Acknowledgment

This work was supported by the Helmholtz Association, project alliance ROBEX, under contract number HA-304. We also thank the many colleagues who have helped us with the logistics involved and the collection of the data.

7 Literature

[1] "ESA Robotics Datasets," https://robotics.estec.esa.int/datasets/all-datasets/, 2018, accessed 15 January 2018.

[2] "ASL Datasets Repository," http://projects.asl.ethz.ch/datasets/doku.php?id=home, 2018, accessed 26 March 2018.

[3] "Datasets," https://projects.asl.ethz.ch/datasets/doku.php?id=related_links, 2018, accessed 26 March 2018.

[4] "OpenSLAM," http://openslam.org/, 2018, accessed 26 March 2018.

[5] R. A. Hewitt, E. Boukas, M. Azkarate, M. Pagnamenta, J. A. Marshall, A. Gasteratos, and G. Visentin, "The katwijk beach planetary rover dataset," *The International Journal of Robotics Research*, vol. 0, no. 0, p. 0278364917737153, 0. [Online]. Available: https://doi.org/10.1177/0278364917737153

[6] M. Woods, A. Shaw, E. Tidey, B. Van Pham, L. Simon *et al.*, "Seeker—autonomous long-range rover navigation for remote exploration," *Journal of Field Robotics*, vol. 31, no. 6, pp. 940–968, 2014. [Online]. Available: http://dx.doi.org/10.1002/rob.21528

[7] A. Wedler, M. Vayugundla, H. Lehner, P. Lehner, M. Schuster *et al.*, "First results of the robex analogue mission campaign: Robotic deployment of seismic networks for future lunar missions," in *68th International Astronautical Congress (IAC)*. Adelaide, Aus-

tralia: International Astronautical Federation (IAF), 25-29 September 2017.

[8] C. Kanzog, "ROBEX - Robotic Exploration of Extreme Environments," http://www.robex-allianz.de/en/, 2018, accessed 12 January 2018.

[9] V. Ciarletti, S. Clifford, A. J. Vieau, B. Lustrement, R. Hassen Khodja, and P. Cais, "Results from the first field tests of the wisdom gpr (2018 exomars mission)," 03 2011.

[10] A. Wedler, B. Rebele, J. Reill, M. Suppa, H. Hirschmüller, C. Brand, M. Schuster, B. Vodermayer, H. Gmeiner, A. Maier, B. Willberg, K. Bussmann, F. Wappler, and M. Hellerer, "Lru - lightweight rover unit," in *Proc. of the 13th Symposium on Advanced Space Technologies in Robotics and Automation (ASTRA)*, May 2015. [Online]. Available: http://robotics.estec.esa.int/ASTRA/Astra2015/

[11] M. J. Schuster, S. G. Brunner, K. Bussmann, S. Büttner, A. Dömel *et al.*, "Towards Autonomous Planetary Exploration: The Lightweight Rover Unit (LRU), its Success in the SpaceBotCamp Challenge, and Beyond," *Journal of Intelligent & Robotic Systems*, Nov 2017. [Online]. Available: https://doi.org/10.1007/s10846-017-0680-9

[12] K. H. Strobl, W. Sepp, S. Fuchs, C. Paredes, M. Smisek, and K. Arbter. DLR CalDe and DLR CalLab. Institute of Robotics and Mechatronics, German Aerospace Center (DLR). Oberpfaffenhofen, Germany. [Online]. Available: http://www.robotic.dlr.de/callab/

[13] M. Fleps, E. Mair, O. Ruepp, M. Suppa, and D. Burschka, "Optimization based imu camera calibration," in *IEEE/RSJ International Conference on Intelligent Robots and Systems*, Sept 2011, pp. 3297–3304.

[14] E. Mair, M. Fleps, M. Suppa, and D. Burschka, "Spatio-temporal initialization for imu to camera registration," in *IEEE International Conference on Robotics and Biomimetics*, Dec 2011, pp. 557–564.

[15] N. Seegmiller and A. Kelly, "Enhanced 3D Kinematic Modeling of Wheeled Mobile Robots," in *Proc. of Robotics: Science and Systems X*, 2014.

[16] H. Hirschmüller, "Stereo processing by semiglobal matching and mutual information," *IEEE Transactions on pattern analysis and machine intelligence*, vol. 30, no. 2, pp. 328–341, 2008.

[17] H. Hirschmüller, P. R. Innocent, and J. M. Garibaldi, "Fast, unconstrained camera motion estimation from stereo without tracking and robust statistics," in *7th International Conference on Control, Automation, Robotics and Vision (ICARCV)*, vol. 2. IEEE, 2002, pp. 1099–1104.

[18] K. Schmid, F. Ruess, and D. Burschka, "Local reference filter for life-long vision aided inertial navigation," in *17th International Conference on Information Fusion (FUSION)*. IEEE, 2014, pp. 1–8.

[19] "RTKLIB: An Open Source Program Package for GNSS Positioning," http://www.rtklib.com/, 2018, accessed 26 March 2018.

ISBN 978-3-8007-4699-6